REPORT DOCUMENTATION PAGE

Form Approved
OMB No. 0704-0188

PLEASE DO NOT RETURN YOUR FORM TO THE ABOVE ORGANIZATION.

1. REPORT DATE *(DD-MM-YYYY)*	2. REPORT TYPE	3. DATES COVERED *(From - To)*
12-07-2007	Journal Article	

4. TITLE AND SUBTITLE

Spectral Signature Wave Breaking in Surface Wave Components of Intermediate Length Scale

5a. CONTRACT NUMBER

5b. GRANT NUMBER

5c. PROGRAM ELEMENT NUMBER

0602435N

6. AUTHOR(S)

Paul A. Hwang

5d. PROJECT NUMBER

5e. TASK NUMBER

5f. WORK UNIT NUMBER

73-6628-85-5

7. PERFORMING ORGANIZATION NAME(S) AND ADDRESS(ES)

Naval Research Laboratory
Oceanography Division
Stennis Space Center, MS 39529-5004

8. PERFORMING ORGANIZATION REPORT NUMBER

NRL/JA/7330-05-5262

9. SPONSORING/MONITORING AGENCY NAME(S) AND ADDRESS(ES)

Office of Naval Research
800 N. Quincy St.
Arlington, VA 22217-5660

10. SPONSOR/MONITOR'S ACRONYM(S)

ONR

11. SPONSOR/MONITOR'S REPORT NUMBER(S)

12. DISTRIBUTION/AVAILABILITY STATEMENT

Approved for public release, distribution is unlimited.

13. SUPPLEMENTARY NOTES

14. ABSTRACT

This paper investigates the length scale of ocean surface breaking waves in the spectral range of intermediate wavelength components a few centimeters to a few meters long. The spectral properties of wave breaking are examined first with the dissipation function of the wave action density conservation equation. The analysis reveals a strong breaking signature in wave components between 0.15 and 1.5 m long in the form of a quasi-singular behavior of the dissipation function using the present formulation of the wind-generation and breaking dissipation functions. Independent studies of more-direct breaking observations of radar tracking of sea spikes in the past have shown close correlation between sea spiked and scatterers traveling at the speed of surface waves a few meters long and much shorter than the dominant wavelength. The intermediate-scale waves are the primary contributor of the ocean surface mean-square slope. the close correlation between the gas transfer rate and the mean-square slope has been demonstrated repeatedly. A better understanding of the wave dynamics of intermediate-scale waves is important for clarification of various gas transfer mechanisms.

15. SUBJECT TERMS

wave breaking, surface roughness, intermediate-length scale, dissipation, sea spikes

16. SECURITY CLASSIFICATION OF:			17. LIMITATION OF ABSTRACT	18. NUMBER OF PAGES	19a. NAME OF RESPONSIBLE PERSON
a. REPORT	b. ABSTRACT	c. THIS PAGE			Paul A. Hwang
Unclassified	Unclassified	Unclassified	UL	10	19b. TELEPHONE NUMBER *(Include area code)* 202-767-0800

Available online at www.sciencedirect.com
ScienceDirect
Journal of Marine Systems 66 (2007) 28–37
JOURNAL OF MARINE SYSTEMS
www.elsevier.com/locate/jmarsys

Spectral signature of wave breaking in surface wave components of intermediate-length scale

Paul A. Hwang *

Bldg. 2, Room 244E, Naval Research Laboratory, 4555 Overlook Avenue SW, Washington, DC 20375, U.S.A.

Received 12 September 2005; accepted 11 November 2005
Available online 7 September 2006

Abstract

This paper investigates the length scale of ocean surface breaking waves in the spectral range of intermediate wavelength components a few centimeters to a few meters long. The spectral properties of wave breaking are examined first with the dissipation function of the wave action density conservation equation. The analysis reveals a strong breaking signature in wave components between 0.15 and 1.5 m long in the form of a quasi-singular behavior of the dissipation function using the present formulation of the wind-generation and breaking dissipation functions. Independent studies of more-direct breaking observations of radar tracking of sea spikes in the past have shown close correlation between sea spikes and scatterers traveling at the speed of surface waves a few meters long and much shorter than the dominant wavelength. This feature of sea-spike properties is consistent with the breaking signature of the dissipation function in similar wavelengths. The intermediate-scale waves are the primary contributor of the ocean surface mean-square slope. The close correlation between the gas transfer rate and the mean-square slope has been demonstrated repeatedly. A better understanding of the wave dynamics of intermediate-scale waves is important for clarification of various gas transfer mechanisms.

Keywords: Wave breaking; Surface roughness; Intermediate-length scale; Dissipation; Sea spikes

1. Introduction

Wave breaking has profound impacts on the upper-ocean turbulence properties, the disruption of the ocean surface cool skin, the generation and entrainment of air bubbles into the water column, and the composition of the ocean surface roughness. All factors cited above are known to produce significant modifications of the gas transfer rate across the air–sea interface (e.g., Phillips, 1985; Wallace and Wirick, 1992; Thorpe, 1993; Melville, 1994; Monahan, 2002; Asher et al., 2002). Clarification of the spectral properties of breaking surface waves may contribute to a better understanding of the gas transfer process in the ocean. Wave breaking is also an important subject in many different ocean remote sensing applications, for example, sea spikes in radar scatter from the ocean surface (e.g., Lee et al., 1996; Frasier et al., 1998; Liu et al., 1998; Phillips et al., 2001) and bubble effects on underwater acoustics (e.g., Ding and Farmer, 1994; Deane and Stokes, 2002; Melville and Matusov, 2002).

In this paper, experimental results on the length scale of breaking waves are examined. Section 2 describes the indirect approach of breaking wave analysis through the investigation of the dissipation function of the wave

* Tel.: +1 202 767 0800; fax: +1 202 767 5599.
E-mail address: phwang@ccs.nrl.navy.mil.

0924-7963/$ - see front matter © 2006 Elsevier B.V. All rights reserved.
doi:10.1016/j.jmarsys.2005.11.015

action density conservation equation (e.g., Phillips, 1984, 1985). The method has been applied to the spectra of intermediate-scale waves (from 0.02 to 6.3 m long) collected in the ocean using a free-drifting measurement technique to mitigate the problem of Doppler frequency shift in converting the measured encounter-frequency spectrum to the wavenumber domain (Hwang and Wang, 2004). Interesting features of the spectral properties of intermediate-scale surface waves in the ocean derived from the analysis are discussed. In Section 3, the wind-speed dependence of the wave spectral density is presented. The topic is of great interest in many areas of research including wave dynamics, air–sea interaction and microwave remote sensing of the ocean. Results from earlier studies on surface waves of length scales from long gravity waves to short capillary waves are found to be in good agreement with the intermediate-scale wave data. In Section 4, the dissipation function derived from the action density conservation equation is described. The most interesting result is that the dissipation function displays a quasi-singular property in the middle range (about 0.15 to 1.5 m) of the intermediate-length scale. Such a feature is interpreted as a distinct signature of wave breaking in wave components of intermediate-length scale. Results on the length scale of wave breaking obtained from more-direct wave breaking measurement techniques, including tracking of bubble-generated acoustic noise (Ding and Farmer, 1994), radar sea spikes (Lee et al., 1996; Liu et al., 1998; Frasier et al., 1998; Phillips et al., 2001), whitecaps (Melville and Matusov, 2002), and high-speed photographs of bubble plume formation (Deane and Stokes, 2002) are investigated in Section 5. It is shown that the length scales of wave breaking derived from direct and indirect methods are in very good agreement. Additional discussions on issues of wave dynamics are given in Section 6 and a summary is presented in Section 7.

2. Analysis

Wave breaking is the dominant dissipation mechanism in the source function balance of the action or energy conservation equation of surface waves. The conservation equation of wave action, $N(\boldsymbol{k})$, can be expressed as (e.g., Phillips, 1984, 1985)

$$\frac{\mathrm{d}N}{\mathrm{d}t} = -\frac{\partial T_i}{\partial \boldsymbol{k}_i} + S_{\mathrm{w}} - D, \tag{1}$$

where $\boldsymbol{k}$ is the wavenumber vector with modulus k. The three terms on the right-hand side of (1) represent the source functions due to nonlinear wave–wave interaction, wind input and breaking dissipation. N is related to the 2D wave displacement spectral density, $\chi(\boldsymbol{k})$, by $N(\boldsymbol{k})=g\chi(\boldsymbol{k})/\sigma$, g the gravitational acceleration, and σ the intrinsic frequency of the wave component. In the following, the result applicable to the omni-directional spectrum, $\chi(k)=\int\chi(k)k\mathrm{d}\theta$ and $N(k)=g\chi(k)/\sigma$, is discussed.

Theoretical and experimental studies of the energy transfer from wind to waves have led to the following parameterization function for the wind input source function (Plant, 1982; Phillips, 1984)

$$S_{\mathrm{w}}(k) = m\sigma\left(\frac{u_*}{c}\right)^2 N(k), \tag{2}$$

where $m\approx 0.04$. For gravity waves several times shorter than the spectral peak component, the nonlinear wave–wave interaction term is much smaller than the other two terms (Phillips, 1977, 1984). The dynamic balance of intermediate- and short-scale gravity waves, therefore, is mainly determined by the wind-input and breaking dissipation terms. Phillips (1984, 1985) suggested the following expression for the omni-directional dissipation sink term

$$D = gk^{-3}f(B), \tag{3}$$

where $B=k^3\chi=k^3\sigma N/g$ is the dimensionless wave spectrum representing the degree of saturation (Phillips, 1985). Eq. (2) can be expressed in terms of B,

$$S_{\mathrm{w}}(k) = m\left(\frac{u_*}{c}\right)^2 gk^{-3}B(k). \tag{4}$$

At equilibrium $\mathrm{d}N/\mathrm{d}t=0$. Equating (3) and (4), Phillips (1984) concluded that the solution to the unknown dissipation function $f(B)$ relies on the knowledge of the dependence of B on the wind speed. Experimental data show that the dependence of the spectral density on wind speed can be represented by a power-law function (Hwang and Wang, 2004)

$$B\left(\frac{u_*}{c}\right) = A_0\left(\frac{u_*}{c}\right)^{a_0}. \tag{5}$$

Assuming a power-law relation for the unknown function in the dissipation term (Phillips, 1984, 1985)

$$f(B) = A_{\mathrm{d}}B^{a_{\mathrm{d}}}, \tag{6}$$

the expressions for a_{d} and A_{d} become simply

$$a_{\mathrm{d}} = 1 + \frac{2}{a_0}, \quad A_{\mathrm{d}} = mA_0^{1-a_{\mathrm{d}}}. \tag{7a, b}$$

3. Spectral dependence on wind speed

The approach described above is most suitable for applications in the region of intermediate- and short-scale waves where the magnitude of the nonlinear wave–wave interaction term is much smaller than that of the wind input or the breaking dissipation term. Obtaining reliable measurements of intermediate- and short-scale waves in the ocean is a complicated task. One of the most difficult issues is the Doppler frequency shift that renders the interpretation of the length scale of measured encounter frequency spectrum an uncertain task (Hwang, 2006). This problem can be mitigated by free-drifting operation that provides measurements in a frame moving with the advecting currents that caused the Doppler frequency shift. Phillips (1984) method of analysis described in the last section is applied to the spectra of intermediate-scale waves (wavelengths between 0.02 and 6.3 m) measured in the ocean using wave gauges mounted on a free-drifting platform (Hwang and Wang, 2004). The results show that $B(u_*/c)$ can be represented by a power-law function (5). An example is shown in Fig. 1a.

Recently, laboratory experiments were conducted in the large wind–wave facility at the Institut de Recherche sur les Phenomenes Hors Equilibre (IRPHE), Marseille, France. The wind-generated surface waves are measured by two separate sensor systems. The first system is a two-dimensional scanning laser slope sensor that generates directly the wavenumber spectrum from the spatial images of the surface slopes over an area 0.1 m × 0.1 m. The second system constitutes of thin-wire wave gauges at fixed stations that provide the frequency spectrum of surface waves measured at essentially the same wind fetch as that of the scanning slope sensor system. The laboratory measurements further confirm the robust power-law relationship of $B(u_*/c)$ as illustrated by the examples shown in Fig. 1b. From these field and laboratory data, A_0 and a_0 can be obtained by least-square fitting of the spectral measurements for each wavenumber component. The results are given in Fig. 1c and d, respectively. An interesting feature in the results of A_0 and a_0 is their nonmonotonic dependence on k, as clearly illustrated in the field data. The results from laboratory experiment (all wind-sea conditions) show a similar dependence of A_0 and a_0 on k in the wavenumber range comparable to those of the field data, but because the length scale of laboratory wind-generated waves is much shorter than that in the field, the interesting nonmonotonic feature revealed by the field data cannot be detected in the laboratory results. Also, there is an apparent wavenumber downshift in the cluster of laboratory data derived from temporal measurements by stationary sensors when compared to the result derived from spatial measurements. This is likely due to

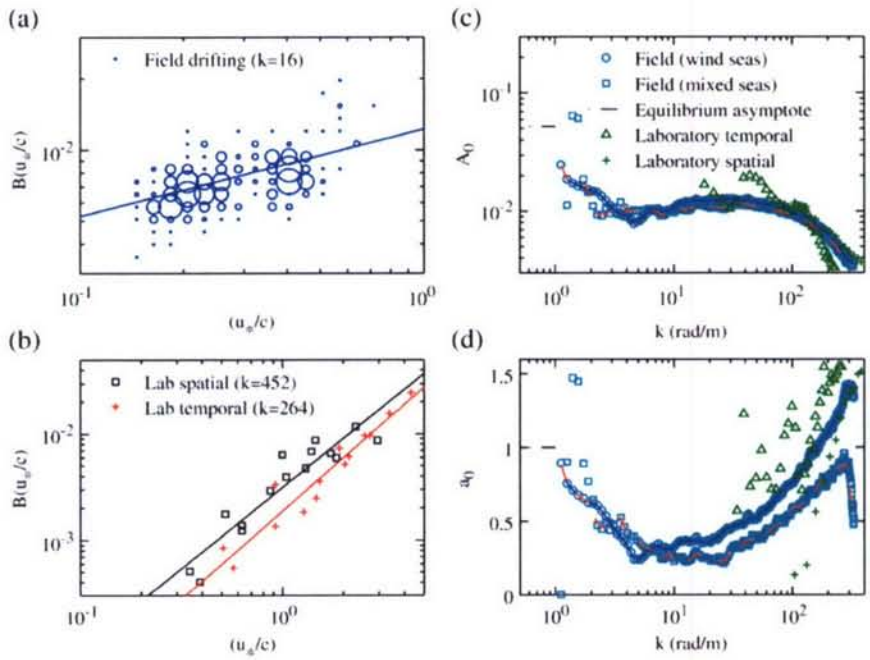

Fig. 1. Examples of the power-law dependence of $B(u_*/c)$: (a) field measurements by wave gauges mounted on a free-drifting platform, (b) laboratory measurements by stationary wave gauges (temporal) and scanning laser slope sensor (spatial). The wavenumber dependence of (c) the proportionality coefficient, A_0, and (d) the exponent, a_0, of the power-law function derived from both field and laboratory experiments.

the Doppler frequency shift induced by the orbital velocity of longer waves. Because the Jacobian connecting the wavenumber-to-frequency conversion is nonlinear with respect to the advecting current, the Doppler frequency shift due to the background orbital velocity does not vanish on averaging over integral cycles of long waves. Instead, the advection by orbital velocity produces a net downshift in the resulting encounter frequency for a given wavenumber component (Hwang, 2006).

The nonmonotonic behavior of the spectral dependence on wind speed as quantified by a_0 is noteworthy. Discussions of this feature have been given by Hwang and Wang (2004) and they are briefly summarized in the following. As illustrated in Fig. 1d, for both conditions of wind sea and mixed sea, the wind speed dependence of the wave spectral density approaches linear toward the long gravity wave region. This is in agreement with many earlier investigations on the wind-speed dependence of the surface wave spectrum in the equilibrium range,

$$\chi_c(k) = bu_* g^{-0.5} k^{-2.5} = b\frac{u_*}{c}k^{-3}. \tag{8}$$

The corresponding dimensionless spectrum is

$$B_c(k) = b\left(\frac{u_*}{c}\right). \tag{9}$$

The range of b varies approximately within a factor-of-two range based on field observations, as has been summarized by many researchers (e.g., Toba, 1973; Phillips, 1985; Forristall, 1981; Donelan et al., 1985; Hwang et al., 2000). Based on the 2D wavenumber spectrum derived from the spatial 3D surface wave topography of a steady and equilibrium wind-generated wave field obtained by an airborne scanning lidar system, Hwang et al. (2000) reported $b \approx 5.26\times10^{-2}$. The analysis of intermediate-scale wave spectra also yields similar values of the proportionality coefficient and exponent (A_0 and a_0) in the lower limit of the resolved wavenumber range ($1 \le k \le 316$ rad/m) (Fig. 1c–d).

Banner et al. (1989) reported wavenumber spectra of surface waves derived from 3D surface topography measured by stereo photography. The resolved wavelengths are between 0.2 and 1.6 m ($31 \ge k \ge 4$ rad/m). The range of wind speeds is between 5.5 and 13.3 m/s. Their results show a very weak wind-speed dependence of the wave spectrum, with $B(k) \sim u_*^{0.18}$ (indicated by a short line-segment in Fig. 2). The analysis of intermediate-scale wave spectra expands the resolved wavelengths to a range from 0.02 to 6.3 m ($1 \le k \le 316$ rad/m). For wind sea, the wind-speed exponent drops sharply from approaching 1.0 (linear) for long gravity waves to about 0.22 near $k=5$ rad/m; a_0 remains to be less than 0.5 through $k=40$ rad/m. In mixed sea, the minimum value of a_0 is also about 0.22, and $a_0 \le 0.3$ for k between 8 and 25 rad/m, and $a_0 \le 0.5$ for k between 3 and 80 rad/m (Fig. 2).

For short gravity waves and capillary waves, field data are usually obtained by radar backscatter measurements

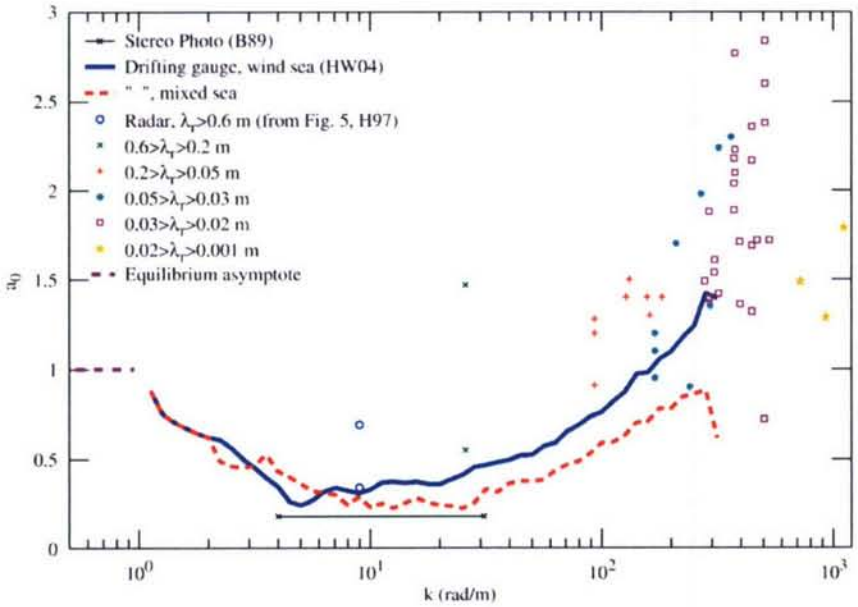

Fig. 2. The wind-speed exponent of a given wave spectral component obtained by different methods including radar return (Jones and Schroeder, 1978; Stewart, 1985; Masuko et al., 1986; Phillips, 1988; Weissman et al., 1994; Colton et al., 1995; summarized in Fig. 5 of Hwang, 1997), stereo photography (Banner et al., 1989), and free-drifting wave gauge (Hwang and Wang, 2004); λ_r is the radar wavelength.

using different radar frequencies and incident angles (e.g., Jones and Schroeder, 1978; Stewart, 1985; Masuko et al., 1986; Phillips, 1988; Weissman et al., 1994; Colton et al., 1995). Fig. 5 of Hwang (1997) summarized the radar data with incidence angles between 25° and 60°, in which range the dominant scattering mechanism is the Bragg resonance so the radar cross section is proportional to the spectral density of the resonant roughness spectral component. The radar data are shown in Fig. 2 together with the result derived from the analysis of intermediate-scale wave spectra described above. Despite the large scatter in the radar data, there are apparent similarities in the results obtained by these fundamentally different approaches of obtaining the wind-speed exponent of the wave spectral component.

4. Dissipation function

Fig. 3 shows the coefficients (7) of the dissipation function (6) obtained from field and laboratory measurements. The breaking dissipation function displays a quasi-singular behavior in the neighborhood of meter-long wave components. In mixed sea, the breaking scale shifts toward smaller breaker size and the size range expands in comparison with those of the wind sea, reflecting the modification by long waves and interaction between background orbital velocity and short waves. The results suggest that the spectral signature of wave breaking is localized in the wavenumber space in the intermediate-length scale. [Detailed breaking wave observations also show the obvious signature at the dominant-wave length scale (e.g., Banner et al., 2000, 2002). The results presented here do not resolve wavelengths near the spectral peak component. The focus of the present research is on surface waves in the intermediate-length scale. These intermediate-scale waves contribute more than 78% to the total mean-square slope of gravity waves generated by winds up to 20 m/s (Hwang, 2005).] From the point-of-view of the spectral response to wind input, as shown in Fig. 1d or Fig. 2, the presence of a localized region in the wavenumber space where the spectral density is only weakly dependent on the forcing wind condition suggests a localized region where the wave growth is quenched by strong dissipation. Further discussions of this point will be described in Section 6. The range of wavelengths with $a_0<0.3$ is about $0.15\leq\lambda\leq1.5$ m. These wave components are sufficiently long such that the energy loss due to viscous dissipation (Lamb, 1945) or generation of parasitic capillary waves (Longuet-Higgins, 1992, 1995) may be neglected. It is reasonable to assume that wave breaking is the major dissipation mechanism for the observed peculiarity in the dissipation function of intermediate-scale waves.

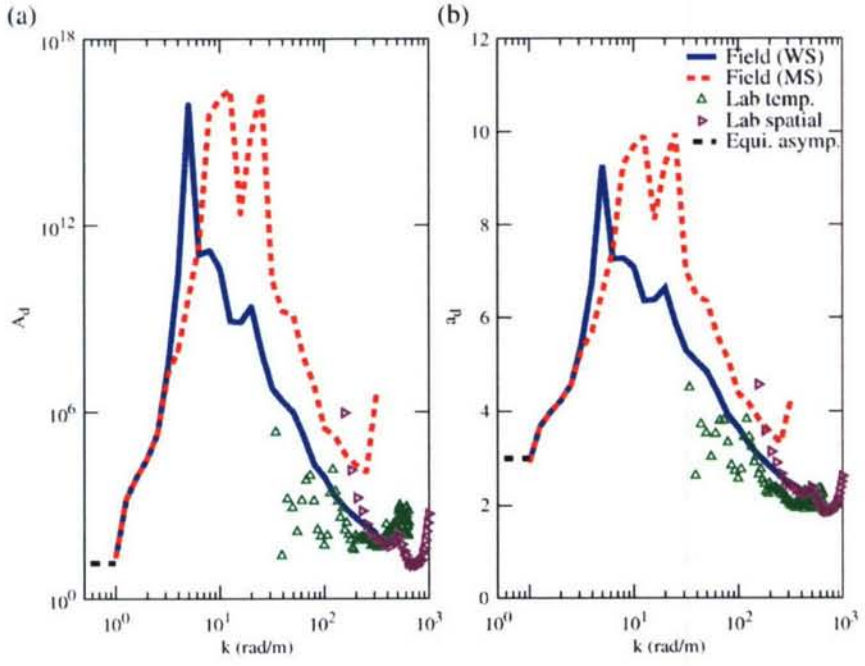

Fig. 3. The wavenumber dependence of (a) the proportionality coefficient, A_d, and (b) the exponent, a_d, of the power-law representation of the dissipation function, $f(B)$. Results from free-drifting measurements in the field in wind sea and mixed sea as well as laboratory data by stationary temporal and spatial measurements are presented.

Microwave observations of the ocean surface over the last few decades indicate that Doppler shifts at HH (horizontal transmitting, horizontal receiving) polarization and low grazing angles are due to scatterers traveling at the speed of surface waves of a few meters long (e.g., Lee et al., 1996; Frasier et al., 1998; and the references therein). This feature is consistent with the strong signature of wave breaking in the intermediate-length wave components. In the next section, some recent breaking-wave observations made by more-direct measurement techniques are summarized to compare with the result using the indirect approach of dissipation-function analysis.

5. Breaking length scale

In the last decade or so, many more-direct measurements of breaking waves have been reported, using techniques such as passive acoustic tracking of the ambient noise produced by bubbles generated by breaking waves (Ding and Farmer, 1994), radar tracking of sea spikes (Lee et al., 1996; Frasier et al., 1998; Liu et al., 1998; Phillips et al., 2001), and video tracking of whitecap evolution (Melville and Matusov, 2002). These remote sensing techniques usually process a very large population of breaking events, on the order of tens of thousands. From these analyses, the authors report statistics of the frequency of occurrences of breaking events as a function of the breaker phase speed. The length scales of breaking waves can be calculated from the reported statistics, they range from about 0.1 to 3 m at 4 m/s wind speed and from 3 to 20 m at 15 m/s wind speed (Fig. 4a). Two major factors contribute to the observed wide range of the breaking length scales at a given wind speed. The first is the dynamic range of the sensors. In particular, the passive acoustic tracking of breaking events cannot detect small-scale breakings due to the problem of ambient noise (Ding and Farmer, 1994). The second factor is the stage of wave development. The experiments reported by Lee et al. (1996) were conducted in a lake and a protected bay with limited wind fetch so the wave field is relatively young compared to the wave conditions of the others obtained in the open ocean environment. The second factor can be compensated somewhat by normalizing the breaking length scale, λ_b, by the dominant wavelength of the wave field, λ_p. With this normalization, the majority of radar data are clustered in the λ_b/λ_p range between 0.04 and 0.2 over the full range of wind speeds encountered in the experiments (Fig. 4b). The mean value with a standard deviation is $\lambda_b/\lambda_p = 0.092 \pm 0.051$, thus the representative breaking length scale is about one order of magnitude shorter than the dominant wavelength of the wave field based on sea-spike observations. [Although the normalized breaking length scale seems to bring together data sets from very

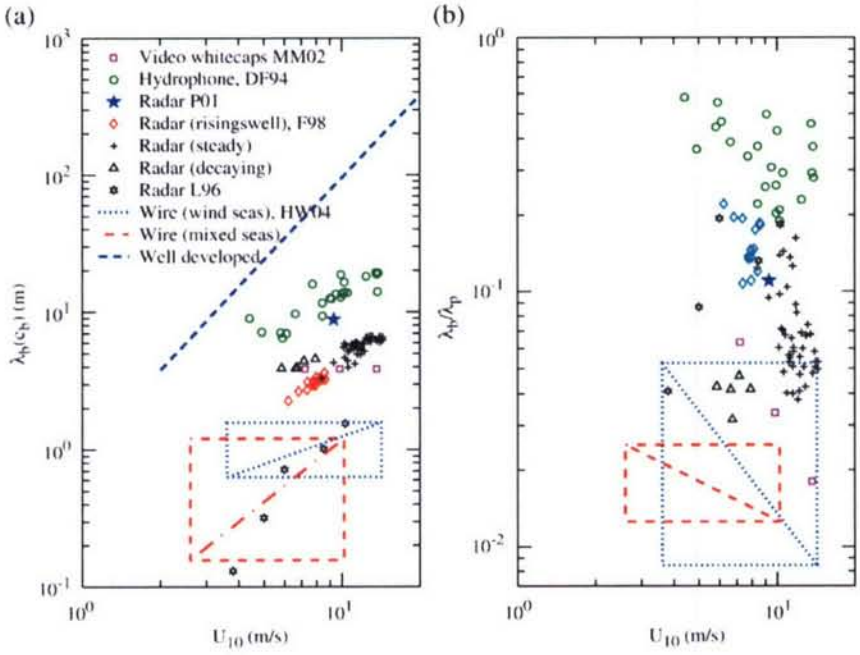

Fig. 4. (a) The representative breaking length scale, λ_b, obtained by different more-direct measurement techniques of wave breaking including tracking of acoustic noise, whitecaps and sea spikes. Estimation of the upper and lower bounds of the breaking length scales from the dissipation analysis is graphed as boxes. (b) Dimensionless breaking length scale, λ_b/λ_p.

different wave development stages, it should be pointed out that for open ocean measurements the data scatter with breaking length given in dimensional form is much smaller than that given in dimensionless form (Fig. 4). The cause and significance of this interesting result is not obvious at this stage but it seems to suggest that the peak wavelength is not necessarily the proper scaling factor for intermediate-length wave components several times shorter than the spectral peak wavelength. If the scaling length is the wavelength at minimum phase speed (determined by the ratio of the gravitational acceleration and the surface tension divided by the water density, and is almost constant in sea water without surface slicks), the reduced scatter in the dimensional representation of the breaking length scale would be sensible. However, as discussed earlier, the range of the length scales of nonmonotonic behavior is between 0.15 and 1.5 m, and far away from the capillary influence. A better explanation remains elusive.]

The breaking length scale can be estimated from the indirect breaking analysis using the dissipation function by setting a threshold in the result of $A_d(k)$ or $a_d(k)$

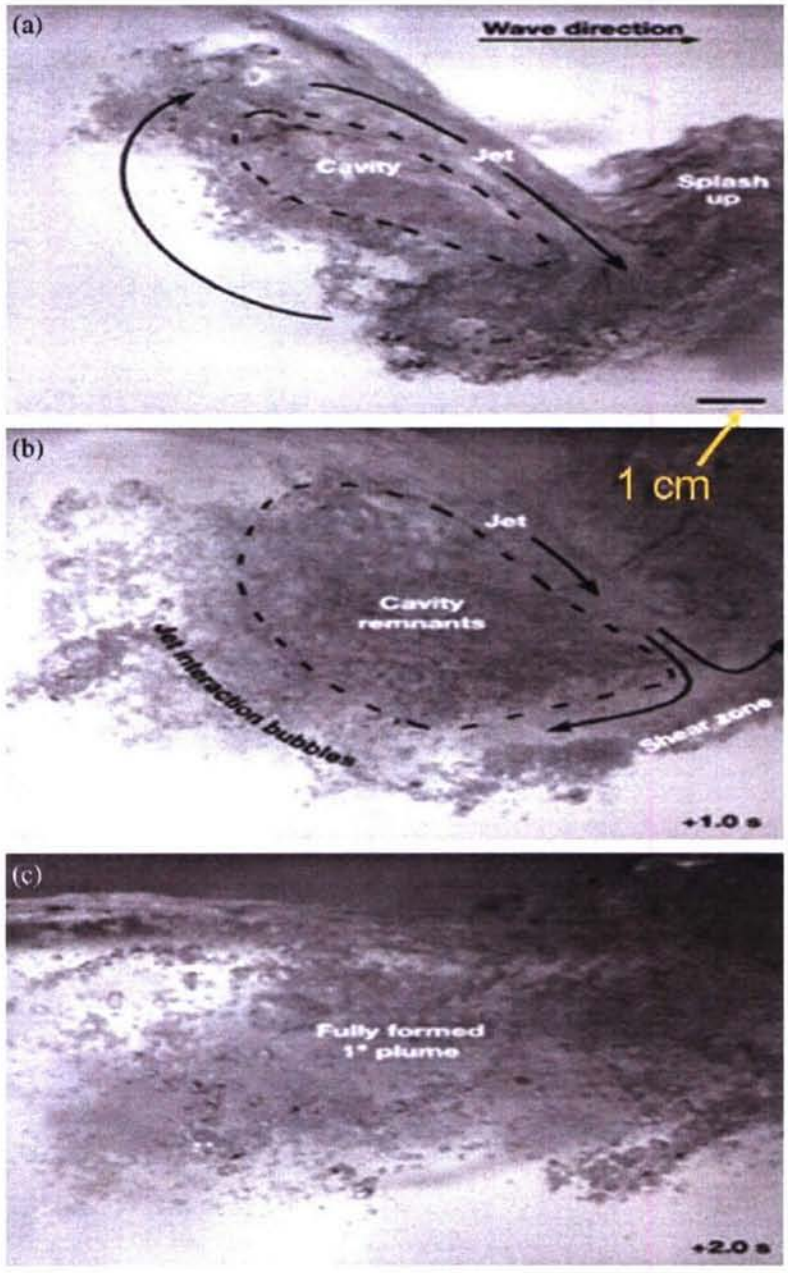

Fig. 5. Pictures from high-speed photography of bubble plume formation under breaking waves (Fig. 2 of Deane and Stokes, 2002).

shown in Fig. 3. For example, applying a threshold of 10^6 times less than the peak value of A_d, one can derive the breaking length scales from the lower and upper bounds of the wave numbers that A_d exceeds the threshold. The result is shown in Fig. 4. The breaking length, λ_b, is between 0.6 and 1.5 m for wind sea, and between 0.15 and 1.2 m for mixed sea. The ratio λ_b/λ_p ranges between 0.013 and 0.025 for wind sea, and from 0.008 to 0.05 for mixed sea. Similar results can be derived by using a threshold (of about 7) in a_d. These values of breaking length scales are smaller than those derived from sea-spike measurements. It is likely that sea-spike tracking overestimates the breaking length scale because the tracking procedure requires a finite dwell time of the breaking event in the field of measurements. For example, Frasier et al. (1998) set a threshold of 1-s minimal dwell time for the sea-spike event to be included in the breaking analysis, thus excluding shorter breaking events in the final statistics. This problem is similar to the ambient-noise limitation on the length-scale resolution in the acoustic tracking of breaking-induced acoustic signature encountered by Ding and Farmer (1994). Taking this bias into consideration, it is concluded that the results from direct and indirect measurements of the breaking length scales are comparable.

Deane and Stokes (2002) conducted laboratory study on the generation mechanism of bubble plumes under breaking waves. Using high-speed photography, they captured many interesting hydrodynamic processes in the active phase of wave breaking. Relevant to the present study is the sequence of pictures depicting the development of bubble plume in the first two seconds after formation of the air cavity trapped by the breaking jet (their Fig. 2, reproduced as Fig. 5 here). The dominant frequency of the wave field is 0.73 Hz and the corresponding wavelength is 2.3 m. As illustrated by the sequence of pictures, after more than one wave period following the formation of the air cavity produced by the jet of wave breaking, the length scale of the active breaking region with intensive dissipation (the vortex regions in the photographs) remains on the order of 0.1 m. This gives an estimate of the ratio $\lambda_b/\lambda_p \approx 0.025$, which is in very good agreement with the results derived from the analysis of the dissipation function shown in Fig. 4b.

6. Discussions

Investigation of the breaking dissipation function is of great interest to many areas of research ranging from ocean and coastal engineering, wave dynamics, air–sea interaction, remote sensing, and numerical wave models. In most applications, the action density conservation equation formulated as Eq. (1) is sufficient. In coastal areas, the bottom dissipation function needs to be included on the right-hand side of the equation. For intermediate-scale waves, the situation is not as clear. A key question is whether wind forcing is the sole source of wave generation. The results from radar sea-spike analyses are very instructive. Many of those experiments are accompanied with detailed video recording of the wave field in the radar field-of-view (e.g., Frasier et al., 1998; Liu et al., 1998). The close association of sea spikes with (large-scale, or dominant) wave breaking or steep waves is convincingly established, yet the phase velocity of the breakers derived from tracking sea spikes is much slower than the phase speed of the dominant wave component. The logical explanation of this result is in the distinction of wave breaking events (as in dominant wave breaking) vs. breaking patches (as in sea spikes or the length scale of the dissipation function). The breaking patches are obviously generated by breaking of dominant waves. For a very short moment, they retain a phase speed close to or exceeding that of the dominant waves (as a bound-wave component). Judging from the sea-spike tracking analysis, this duration is very short and for the remaining part of the sea-spike (breaking) lifetime, the breaking patches propagate as free waves with phase velocities according to their sizes (in the intermediate-length scale). In other words, breaking plays double roles in the intermediate-scale wave components: it is a dissipation function of wave energy ***and*** an important ***source*** function of intermediate-scale wave generation.

Although it is reasonable to state that there is an additional source function due to breaking-wave generation in the intermediate-scale spectral components, it remains a difficult task explaining the lack of response to wind-forcing in the mid-range components of intermediate-scale waves, observed by both in situ wave measurements and remote-sensing radar scatter analyses (Fig. 2). It is generally accepted that breaking probability increases with the cube of wind speed, so incorporation of breaking as a generation term for intermediate-scale waves should increase the wind-speed exponent for the wave components affected, contradicting to the observations of decreased wind-speed exponent in the middle range of the intermediate-length wave components. It remains a tough challenge to explain the observed peculiar nonmonotonic behavior of the spectral properties of intermediate-scale wave components shown in Fig. 2.

Eq. (1) is obviously inadequate for describing the dynamics of intermediate-scale waves. While it worked

nicely for identifying the breaking length scales, it is emphasized that the proposed local balance of breaking dissipation and wind generation functions is a **hypothesis** that leads to the prediction of enhanced dissipation in the intermediate-length wave components. Furthermore, in side-by-side comparison of radar images of sea spikes and video images of ocean surface waves, it was found that the majority of sea-spike events are associated with steep waves without visible breaking whitecaps – approximately 60% for the young and the developed sea and 92% for decaying sea (Liu et al., 1998). It is not clear whether these sea-spike-associated steep waves were undergoing microscale breaking, so an unequivocal causal link between sea spikes and breaking waves is yet to be established. The observations described above are supportive but not conclusive and further observations of enhanced breaking at the intermediate- and short-scale waves are needed to substantiate this prediction conclusively.

7. Summary

Properties of wave breaking can be investigated through the dissipation function of the wave action conservation equation. Following an approach described by Phillips (1984), the functional dependence of $B(u_*/c)$ is found to follow closely the power-law relationship based on data obtained from both field and laboratory environments. The exponent of the power-law, a_0, represents the wind-speed dependence of the spectral wave components. Results from field data that resolve wavelengths between 0.02 and 6.3 m reveal a nonmonotonic behavior of a_0 as a function of k. The spectral densities of wave components between 0.15 and 1.5 m long depend only weakly on the forcing wind condition. The dissipation function displays a quasi-singular behavior in the corresponding wavelength range, suggesting a localized region in the wavenumber domain with a strong breaking signature. This result is consistent with extensive observations of radar sea spikes during the last few decades showing a close correlation between sea spikes and ocean surface scatterers traveling at the speed of surface waves a few meters long. The strong signature of breaking waves in the decimeter- to meter-long waves reflects the important impact of wave breaking on the dynamics of intermediate-scale ocean surface waves that are the major contributor to the ocean surface roughness (Hwang, 2005). The close correlation between the gas transfer velocity and the ocean surface roughness (mean-square slope) has been demonstrated repeatedly. A better understanding of the properties of wave breaking in intermediate-scale spectral components can lead to a better understanding of the gas transfer processes.

Acknowledgements

This work is supported by the Office of Naval Research (Naval Research Laboratory PE61153N and PE62435N). NRL Contribution JA-7330-05-5262.

References

Asher, W., Edson, J., McGillis, W., Wanninkhof, R., Jo, D.T., Litchendorf, T., 2002. Fractional area whitecap coverage and air–sea gas transfer velocities measured during GasEx-98. In: Donelan, M.A., Drennan, W.M., Saltzman, E.S., Wanninkhof, R. (Eds.), Gas Transfer at Water Surfaces. AGU Press, pp. 199–203.

Banner, M.L., Jones, I.S.F., Trinder, J.C., 1989. Wavenumber spectra of short gravity waves. J. Fluid Mech. 198, 321–344.

Banner, M.L., Babanin, A.V., Young, I.R., 2000. Breaking probability for dominant waves on the sea surface. J. Phys. Oceanogr. 30, 3145–3160.

Banner, M.L., Gemmrich, J.R., Farmer, D.R., 2002. Multiscale measurements of ocean wave breaking probability. J. Phys. Oceanogr. 32, 3364–3375.

Colton, M.C., Plant, W.J., Keller, W.C., Geernaert, G.L., 1995. Tower-based measurements of normalized radar cross section from Lake Ontario: evidence of wind stress dependence. J. Geophys. Res. 100, 8791–8813.

Deane, G.B., Stokes, M.D., 2002. Scale dependence of bubble creation mechanisms in breaking waves. Nature 418, 839–844.

Ding, L., Farmer, D.M., 1994. Observations of breaking surface wave statistics. J. Phys. Oceanogr. 24, 1368–1387.

Donelan, M.A., Hamilton, J., Hui, W.H., 1985. Directional spectra of wind-generated waves. Philos. Trans. R. Soc. Lond., A A315, 509–562.

Forristall, G.Z., 1981. Measurements of a saturated range in ocean wave spectra. J. Geophys. Res. 86, 8075–8084.

Frasier, S.J., Liu, Y., McIntosh, R.E., 1998. Space–time properties of radar sea spikes and their relation to wind and wave conditions. J. Geophys. Res. 103, 18745–18757.

Hwang, P.A., 1997. A study of the wavenumber spectra of short water waves in the ocean: Part 2. Spectral model and mean square slope. J. Atmos. Ocean. Technol. 14, 1174–1186.

Hwang, P.A., 2006. Doppler frequency shift in ocean wave measurements: frequency downshift of a wavenumber component by advection of background wave orbital velocity. J. Geophys. Res. 111, C06033.

Hwang, P.A., 2005. Wavenumber spectrum and mean-square slope of intermediate-scale ocean surface waves. J. Geophys. Res. 110, C10029. doi:10.1029/2005JC003002.

Hwang, P.A., Wang, D.W., 2004. An empirical investigation of source term balance of small scale surface waves. Geophys. Res. Lett. 31, L15301. doi:10.1029/2004GL20080.

Hwang, P.A., Wang, D.W., Walsh, E.J., Krabill, W.B., Swift, R.N., 2000. Airborne measurements of the directional wavenumber spectra of ocean surface waves: Part 1. Spectral slope and dimensionless spectral coefficient. J. Phys. Oceanogr. 30, 2753–2767.

Jones, W.L., Schroeder, L.C., 1978. Radar backscatter from the ocean: dependence on surface friction velocity. Boundary - Layer Meteorol. 13, 133–149.

Lamb, H., 1945. Hydrodynamics, 6th ed. Dover Publications, New York. 738 pp.

Lee, P.H.Y., Barter, J.D., Caponi, E., Caponi, M., Hindman, C.L., Lake, B.M., Rungaldier, H., 1996. Wind-speed dependence of small-grazing-angle microwave backscatter from sea surfaces. IEEE Trans. Antennas Propag. 44, 333–340.

Liu, Y., Frasier, S.J., McIntosh, R.E., 1998. Measurement and classification of low-grazing-angle radar sea spikes. IEEE Trans. Antennas Propag. 46, 27–40.

Longuet-Higgins, M.S., 1992. Capillary rollers and bores. J. Fluid Mech. 240, 659–679.

Longuet-Higgins, M.S., 1995. Parasitic capillary waves: a direct calculation. J. Fluid Mech. 301, 79–107.

Masuko, H., Okomoto, K., Shimada, M., Niwa, S., 1986. Measurement of microwave backscattering signatures of the ocean surface using X-band and K_u-band airborne scatterometers. J. Geophys. Res. 91, 13065–13083.

Melville, W.K., 1994. Energy dissipation by breaking waves. J. Phys. Oceanogr. 24, 2041–2049.

Melville, W.K., Matusov, P., 2002. Distribution of breaking waves at the sea surface. Nature 417, 58–63.

Monahan, E.C., 2002. The physical and practical implications of a CO_2 gas transfer coefficient that varies as the cube of the wind speed. In: Donelan, M.A., Drennan, W.M., Saltzman, E.S., Wanninkhof, R. (Eds.), Gas Transfer at Water Surfaces. AGU Press, pp. 193–197.

Phillips, O.M., 1977. The Dynamics of the Upper Ocean, 2nd ed. Cambridge Univ. Press. 336 pp.

Phillips, O.M., 1984. On the response of short ocean wave components at a fixed wavenumber to ocean current variations. J. Phys. Oceanogr. 14, 1425–1433.

Phillips, O.M., 1985. Spectral and statistical properties of the equilibrium range in wind-generated gravity waves. J. Fluid Mech. 156, 505–531.

Phillips, O.M., 1988. Radar return from the sea surface – Bragg scattering and breaking waves. J. Phys. Oceanogr. 18, 1065–1074.

Phillips, O.M., Posner, F.L., Hansen, J.P., 2001. High range resolution radar measurements of the speed distribution of breaking events in wind-generated ocean waves: surface impulse and wave energy dissipation rates. J. Phys. Oceanogr. 31, 450–460.

Plant, W.J., 1982. A relationship between wind stress and wave slope. J. Geophys. Res. 87, 1961–1967.

Stewart, R.H., 1985. Method of Satellite Oceanography. University of California Press. 360 pp.

Thorpe, S.A., 1993. Energy loss by breaking waves. J. Phys. Oceanogr. 23, 2498–2502.

Toba, Y., 1973. Local balance in the air–sea boundary processes: III. On the spectrum of wind waves. J. Phys. Oceanogr. 3, 579–593.

Wallace, D.W.R., Wirick, C.D., 1992. Large air–sea gas fluxes associated with breaking waves. Nature 356, 694–696.

Weissman, D.E., Davidson, K.L., Brown, R.A., Friehe, C.A., Li, F., 1994. Relationship between the microwave radar cross section and both wind speed and stress: model function studies using Frontal Air–Sea Interaction Experiment data. J. Geophys. Res. 99, 10087–10108.